IET Science, Measurement & Technology

*Research Article*

IET Journals
The Institution of Engineering and Technology

# In-vitro study of human proximal femur microstructure: analysis of the relationship between micro-computed tomography data and quantitative ultrasound parameters

ISSN 1751-8822
Received on 18th March 2015
Revised on 2nd October 2015
Accepted on 1st December 2015
doi: 10.1049/iet-smt.2015.0041
www.ietdl.org

*Marco Peccarisi[1], Tommaso De Marco[1], Francesco Conversano[2], Paola Pisani[2], Luigi Spedicato[1], Antonio Greco[1], Daniele Panetta[2], Giulio Guido[3], Vanna Bottai[3], Piero A. Salvadori[2], Sergio Casciaro[2]* ✉

[1]*Echolight Srl, Lecce, Italy*
[2]*National Research Council, Institute of Clinical Physiology, Lecce-Pisa, Italy*
[3]*Clinical Orthopaedics and Traumatology II, University of Pisa, Pisa, Italy*
✉ *E-mail: sergio.casciaro@cnr.it*

**Abstract:** The aim of this study was to investigate the relationships between selected quantitative ultrasound (QUS) parameters and human femur microstructure properties, as quantified by micro-computed tomography (micro-CT). The authors employed an innovative custom-designed experimental set-up, which allowed the insonification of each portion of an excised femoral head sample, simultaneously including trabecular region, cortical layer and cartilage in their physiologic morphological configuration. Thirty different, uniformly distributed, regions of interest were analysed for the calculation of apparent integrated backscatter (AIB), integrated reflection coefficient (IRC) and several micro-CT parameters. QUS data acquisitions were performed through both single-element ultrasound transducers at two different frequencies (2.25 and 3.5 MHz) and a clinically available 128-element echographic probe. Obtained results showed that AIB was strongly correlated with trabecular network properties ($|r|$ up to 0.80) and IRC had appreciable linear correlations with cortical bone density ($|r|$ up to 0.57). The agreement between single-element transducers and echographic probe, combined with the innovative approach of considering the entire femoral head in its physiological shape with all its components (cartilage, cortical layer, trabecular region), encourages the clinical translation of the proposed approach as a possible new method for early osteoporosis diagnosis.

## 1 Introduction

Osteoporosis and its related fractures are becoming an important public health problem, since they represent a very heavy economic burden for national healthcare systems [1]. In fact, osteoporotic fractures and their complications cause a reduced quality of life and an increased mortality rate for osteoporotic patients [2].

The key to an effective prevention is the adoption of simple and inexpensive methods for population mass screenings [3, 4]. Currently, the 'gold standard' method for osteoporosis diagnosis is the measurement of bone mineral density through dual X-ray absorptiometry (DXA) [5–10]. Unfortunately, this kind of densitometry has some important limitations, mainly related to X-ray exposure and the associated risks [11–14], high costs and limited availability, that hinder its use for mass screening purposes [3, 4, 15, 16]. Moreover, the typical DXA investigation cannot provide information on bone microarchitecture, unless the DXA scanner is equipped with a recently developed software package for the calculation of the so-called 'trabecular bone score' [17, 18], whose additional installation represents anyway a further cost increment.

The employment of quantitative ultrasound (QUS) methods, which are intrinsically more prone to detect bone microarchitecture properties, is an alternative to DXA that is attracting an increasing interest because of its several potential advantages, such as absence of ionising radiation exposure, portable machines, lower costs and wider availability [5, 16, 19]. In fact, bone health assessment is just one out of the several biomedical applications of ultrasound (US) systems that have been introduced in the last years because of their mentioned intrinsic advantages over competing technologies [20–30].

Several QUS parameters have been proposed in literature in order to extract useful diagnostic information from the interaction between US waves and human bones [19, 31–33]. Among those already available in clinical routine, the most common QUS parameters are currently derived from devices employing through-transmission measurements at the calcaneus, including broadband US attenuation, speed of sound and stiffness index [34–36]. Recent experimental studies have also documented the potential of US backscattering as an innovative and promising technique for osteoporosis diagnosis through parameters such as backscatter coefficient [37], apparent integrated backscatter (AIB) [38–41], frequency slope of apparent backscatter and time slope of apparent backscatter [38], spectral centroid shift [39], broadband US backscatter [40], integrated reflection coefficient (IRC) [40, 41], mean of the backscatter difference spectrum and slope of the backscatter difference spectrum [42].

In this context, in a recent conference paper [43] we presented an in-vitro characterisation of human proximal femur microstructure through QUS backscatter parameters, evaluated in comparison with micro-computed tomography (micro-CT) data. The referred study [43] was conducted employing an innovative custom-designed experimental set-up that allowed the possibility of insonifying each portion of an excised femoral head, including both the trabecular region and the cortical layer in their physiologic morphological configuration. The peculiarity of this approach consisted in employing the entire femoral head instead of suitably shaped samples of pure trabecular bone tissue, which is the typically adopted approach in previous literature-available papers [37, 38, 42, 44]: our strategy represented a step forward towards the possible clinical translation of the proposed methodology. The reported preliminary results were obtained on a

femoral head sample insonified employing a 2.25 MHz mono-element unfocused US transducer.

In the present work, we performed a more accurate characterisation of the femoral head sample by insonifying and analysing 30 different regions of interest (ROIs) uniformly distributed throughout the considered target volume, in place of the 22 non-uniformly distributed ROIs that had been considered in our previous investigation. Two different US frequencies (2.25 and 3.5 MHz) were also used, in order to evaluate possible frequency dependencies of obtained results. Furthermore, in the final part of the study, a modified experimental set-up was adopted in order to allow the employment of a conventional clinically available convex echographic probe, with the aim of evaluating the actual employability of the proposed approach and facilitating its clinical translation.

## 2 Materials and methods

### 2.1 Bone sample

A femoral head sample was obtained from a patient who had undergone surgery for prosthesis implant following a coxarthrosis diagnosis. The extracted bone sample was immersed in formalin (4% v/v) immediately after excision and stored in a sealed container until the execution of the US and micro-CT scans described in the next paragraphs.

### 2.2 US acquisitions

*2.2.1 Single-element transducers:* In the first part of the study, the adopted experimental set-up for US data acquisition through single-element transducers was the same that has been described in detail in our previous work [43]. A picture of the employed set-up is reported in Fig. 1 and its main characteristics are briefly reported herein.

The bone sample was drilled along the head-neck axis and a screw was carefully threaded into the realised hole (see Fig. 1). The screw was in turn linked to a mechanical system that allowed, by means of a crank handle, the rotation of the sample around its head-neck axis, which could be roughly considered as a kind of 'symmetry axis' of the sample. In this way, it was possible to rotate step-by-step the bone sample and to assure that backscattered US signals came from a specific target slice located at enough distance from the screw hole. The described set-up was placed in a plastic tank and immersed in distilled water at room temperature (20°C). The US transducer, employed in reflection mode, was positioned in such a way as to insonify the bone sample slice corresponding to its largest transversal section, whose profile closely resembled a circular shape (see Fig. 2); consequently, considering that the only possible sample movement was the rotation around its head-neck axis, the distance between the US transducer and the insonified surface could be considered approximately constant.

Sample insonifications were performed considering 30 different rotation angle steps of 12° each (Fig. 2). The sample was insonified twice, each time employing a different single-element unfocused transducer with an external diameter of 16 mm and a capsule diameter of 12.7 mm: the first 30-step insonification was carried out using a 2.25 MHz submersible transducer (V-306-SU, Panametrics, Waltham, MA, USA) and the second insonification using a 3.5 MHz submersible transducer (V-382-SU, Panametrics). The transducer was connected to a pulser receiver (Panametrics PR5077), which generated 400 V pulses centred at the transducer frequency at a pulse repetition rate of 200 Hz. Received backscatter signals were 10 dB amplified and 1 kHz high-pass filtered before being sent to a data-acquisition board (PCI-5122, National Instruments, Austin, Texas, USA) for analogue-to-digital conversion (100 MS/s, 14 bits) and storage on a computer hard-disk.

For each rotation step, 50 signal records, corresponding to the backscattering of 50 incident US pulses, were acquired and averaged in order to improve the signal-to-noise ratio (SNR). For each employed transducer, a reference signal was also acquired by replacing the bone sample with a perfect US reflector, represented by a steel plate.

*2.2.2 Convex echographic probe:* In the second part of the study, a modified version of the US acquisition set-up was used, in order to allow the employment of a clinically available echographic device (Echo Blaster 128, Telemed Medical Systems, Milan, Italy), which was equipped with a 128-element convex probe (C3.5/60/128 Z, Telemed Medical Systems) operating at 3.5 MHz. The device was provided in a research configuration that allowed the acquisition of both conventional B-mode echographic images and 'raw' unprocessed radiofrequency (RF) signals, which were high-pass filtered, amplified, digitised and stored through the same signal pre-processing chain used in the case of single-element US transducers.

The convex probe was partially immersed in the water tank containing the previously described set-up and fixed in such a way as to insonify the bone sample slice corresponding to the largest transversal section of the sample itself, as shown in Fig. 3. Sample insonifications were again performed considering 30 different rotation angle steps of 12°, acquiring 10 frames of RF data for each step. A reference signal was also acquired in this case by replacing the bone sample with a perfect US reflector, consisting of a steel plate.

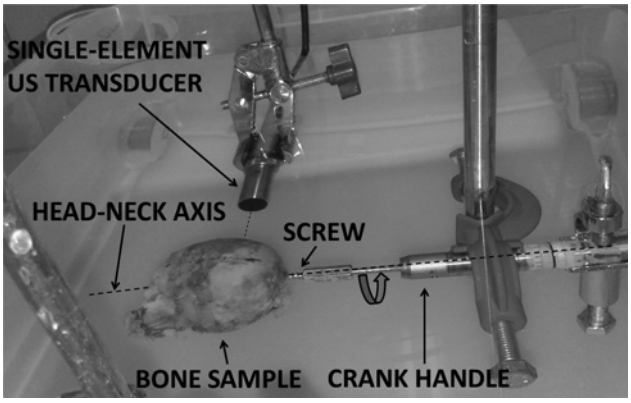


**Fig. 1** *Picture of the experimental set-up adopted for US data acquisitions with a single-element transducer. The set-up was realised in order to allow controlled rotations of the bone sample around its head-neck axis*

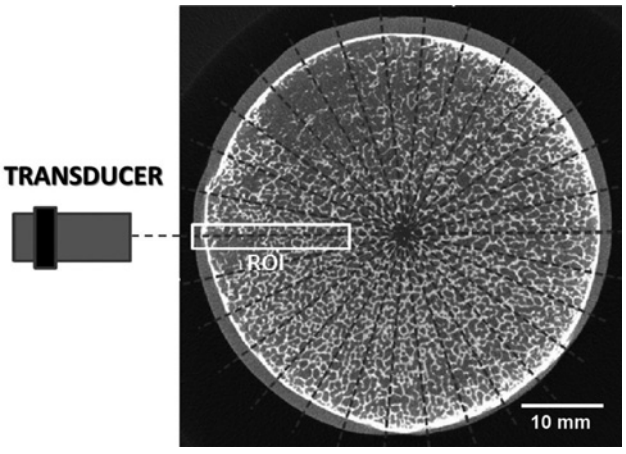


**Fig. 2** *Micro-CT image of the transverse plane of the bone sample. The 30 US insonification directions are indicated by the dotted lines; for each direction a specific ROI was considered, as defined by the rectangular box for the selected direction. For each ROI, the parameters extracted from the corresponding US signal were compared with the micro-CT ones calculated in the same ROI*


*IET Sci. Meas. Technol.*, 2016, Vol. 10, Iss. 3, pp. 193–199

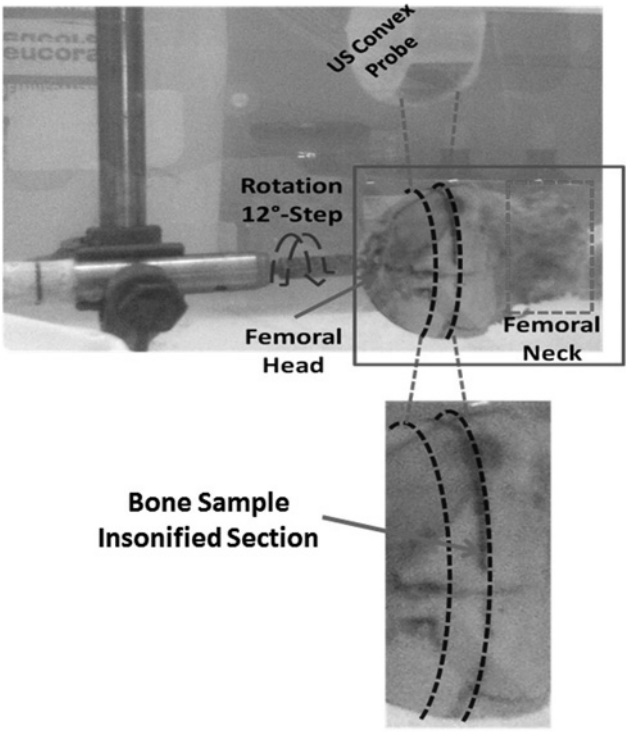


**Fig. 3** *Main details of the experimental set-up adopted for US data acquisitions with the convex probe*

### 2.3 US data analysis

Referring to the single-element transducer acquisitions, for both the considered incident frequencies, IRC and AIB values were calculated from the average US signal acquired for each rotation angle step.

We followed the approach reported in [44] in order to identify the signal portions coming from cartilage, cortical layer or trabecular region: considering the reference signal envelope, two time windows $\Delta T_1 = t_M - t_1$ and $\Delta T_2 = t_2 - t_M$ were defined ($t_M$ represents the time position of signal envelope maximum, while $t_1$ and $t_2$ are the closest points in which envelope amplitude reaches 10% of its peak value). Then, considering the acquisition performed on the bone sample, in each average US signal the ROI corresponding to the cortical region ($ROI_{cort}$) was defined as the union of $\Delta T_1$ and $\Delta T_2$ around the maximum time position $t^*$ in the signal envelope, as shown in Fig. 4. Then the signal portion before $ROI_{cort}$ was attributed to the cartilage; the ROI corresponding to the trabecular region ($ROI_{trab}$) was defined as a time window of 13 µs immediately after $ROI_{cort}$ (the duration of this time window was determined to match the depth of the parallelepipeds considered in the micro-CT data analysis, as detailed in Section 2.4).

Finally, IRC and AIB were computed through the following formulas [45]

$$\mathrm{IRC} = \frac{1}{\Delta f}\int_{\Delta f} 20\log_{10}\left(\frac{A_{\mathrm{cort}}(f)}{A_{\mathrm{ref}}(f)}\right) \mathrm{d}f \tag{1}$$

$$\mathrm{AIB} = \frac{1}{\Delta f}\int_{\Delta f} 20\log_{10}\left(\frac{A_{\mathrm{trab}}(f)}{A_{\mathrm{ref}}(f)}\right) \mathrm{d}f \tag{2}$$

where $A_{cort}$ and $A_{trab}$ represent the amplitude of $ROI_{cort}$ and $ROI_{trab}$ signal spectrum, respectively; $A_{ref}$ is the amplitude of reference signal spectrum and $\Delta f$ is the considered frequency bandwidth, determined as the −6 dB bandwidth of the reference signal spectrum.

Each frame acquired through the convex echographic probe was composed of 253 RF lines, which could, in principle, be processed as the signals acquired through single-element transducers. In our analyses, an 'average RF frame' was preliminary obtained for each considered rotation step by averaging the homologous tracks in the 10-frame acquired sequence. Then, IRC and AIB were calculated for each of the nine central tracks through the same procedure adopted for signals acquired through single-element transducers. The final IRC and AIB values for a given rotation step were obtained by averaging the nine values calculated for the single tracks. The choice of considering just the nine central tracks was motivated by geometrical considerations showing that this was the best approximation in order to have an insonified volume similar to that obtained in the case of single-element transducers.

### 2.4 Micro-CT acquisitions and data analysis

The adopted micro-CT scan protocol was described in our previous work [43] and is briefly recalled herein.

Each bone sample was scanned through a high-resolution micro-CT scanning system (Raytest IRIS micro-PET/CT, Raytest, Straubenhardt, Germany), which performed low-dose acquisitions (80 kV, 1 mA) with isotropic voxels (60 µm).

Subsequent data analysis included 50 micro-CT image slices (16-bit grey level, 886 × 943 voxels), which corresponded to a 3 mm bone thickness centred on maximum sample diameter along the head-neck axis. Thirty parallelepipeds ($3 \times 3 \times 19$ mm$^3$) were extracted from this sub-dataset at the angles shown in Fig. 2. Each parallelepiped contained cartilaginous, cortical and trabecular regions, as illustrated in Fig. 5.

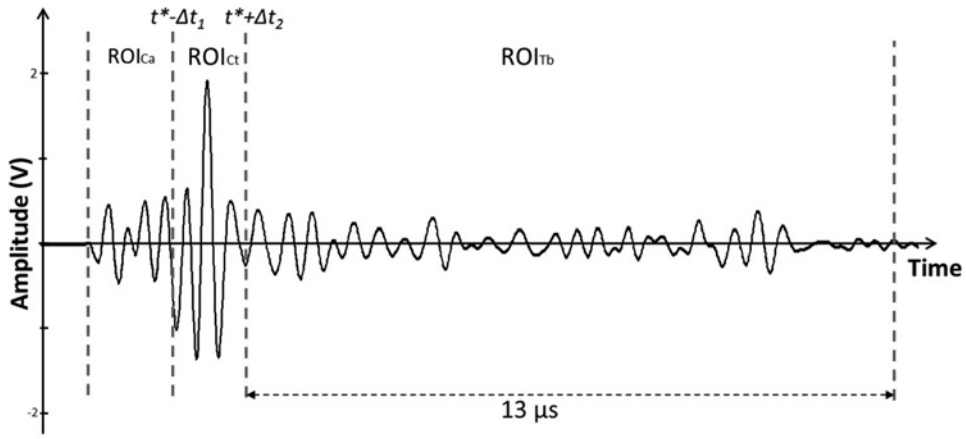


**Fig. 4** *Segmentation of a typical RF signal acquired on the bone sample with a 2.25 MHz single-element transducer. t* is the point where the signal envelope is maximum (not shown in figure). Please see the text for further details*

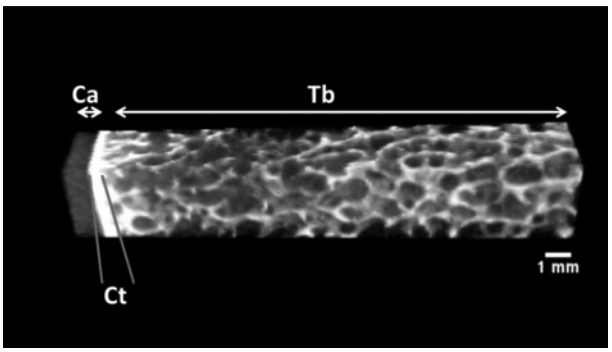


**Fig. 5** *Three-dimensional microstructure of a typical parallelepiped extracted from the micro-CT dataset. Cartilaginous (Ca), cortical (Ct) and trabecular (Tb) regions are indicated*

Size of parallelepiped boxes was established by taking into account that: (i) both the diameter of the US beam generated by single-element transducers and the height of the US beam of the convex probe in the respective focal regions measured ~3 mm, as derived from the corresponding manufacturer data sheets; (ii) preliminary US measurements performed on a different bone sample at the highest employed frequency (3.5 MHz) documented that US signals backscattered from a depth of 19 mm were typically received with a suitable SNR.

The actual US penetration depth was experimentally verified on this second bone sample in the following way. A hole was realised in the bone sample in a direction perpendicular to US propagation, in such a way that the distance between the hole and the sample surface along the US propagation direction was about 19 mm. A screw was then carefully threaded in the realised hole. The variation in the backscattered US signal due to the presence/absence of the screw in the hole identified the time interval corresponding to a 19 mm penetration depth. Afterwards, the insonification of the sample along a different direction (not interested by the hole) allowed the measurement of the SNR at the considered depth. The whole procedure was repeated four times, therefore a total of four holes were realised in the second bone sample and the finally adopted time interval was determined as the average of the corresponding four measurements: taking into account the scheme of RF signal segmentation reported in Fig. 4, we obtained that 13 μs had to be considered after the cortical interface echo, identified by $ROI_{cort}$, in order to match the target penetration depth.

A custom-implemented version of the algorithm reported in [46] was employed for automatic segmentation of cartilaginous, cortical and trabecular volumes on each parallelepiped. BoneJ software [47] was then used to calculate the following structural parameters for cortical and trabecular regions. For the cortical layer, we measured the voxel-based bone volume fraction (BV/TV), representing the volume of mineralised bone per unit volume of the sample. For the trabecular volume, we computed the following parameters: the mean and maximum trabecular bone thickness (Tb.Th Mean and Tb.Th Max, in mm) and spacing (Tb.Sp Mean and Tb.Sp Max, in mm), calculated as in [48]; the structural model index (SMI), which is a parameter that determines the plate-like or rod-like geometry of trabeculae and was calculated following the approach reported in [49]; the bone surface density (BS/TV, in $mm^{-1}$); the fractal dimension, calculated through the box counting method [50]; the connectivity density (Conn.D), representing a measure of the connectivity degree of trabeculae normalised by total volume (TV) [51]; the previously defined voxel-based BV/TV. Cortical thickness was not included in the analysis because, due to the narrow shape of the ROI selected, it did not provide independent information to that already measured by cortical BV/TV.

### 2.5 Statistical analysis

AIB, IRC and micro-CT parameter values were computed for each considered rotation step. The degree of correlation between US and micro-CT measurements was assessed through the corresponding values of Pearson's correlation coefficient. A reproducibility test was also performed, by repeating the same US measurements in the same experimental set-up, which was wholly re-assembled 6 months after the first set of acquisitions. For each considered combination of employed transducer and measured US parameter, the statistical significance of the differences between the mean values of the two sets of US measurements was evaluated using a paired two-tailed Student *t*-test.

## 3 Results and discussion

Obtained mean values of AIB, IRC and micro-CT parameters are shown in Table 1, reporting, for each considered parameter, the average over the 30 rotation steps and the corresponding standard deviation (SD).

Considering the US acquisitions performed through single-element transducers, both AIB and IRC increased with increasing incident US frequency, as expected from previous papers [38, 52]. This means that the ratio between the signal reflected by the sample and the reference one (which represents the total emitted pulse) increases at higher frequencies. Literature-available papers reported for IRC a minor non-systematic increase as a function of frequency [52]; however, those authors considered only suitably shaped samples of pure trabecular bone: in this way IRC calculation resulted mainly influenced by the trabecular porosity. In our approach, instead, we used an intact sample of human femoral head and this consideration may not be fully exhaustive to explain the IRC behaviour, since it was computed from the reflection of the cartilage–cortical bone interface. In our case, the observed effect could be at least partially due to the presence of the cartilaginous layer, which may introduce a selective attenuation of specific US frequencies. This hypothesis would anyway require an experimental confirmation through further studies, employing different frequencies.

Referring to the echographic probe acquisitions, obtained AIB and IRC values resembled those obtained with the single-element transducer having the same centre frequency (3.5 MHz) (Table 1).

Moreover, in order to test the reproducibility of the ultrasonic measurements, the same US acquisitions were performed again by a different operator 6 months after the first experiment. AIB and IRC values were computed for this second measurement set through the same previously employed procedures. The results of the two measurement sets were compared with each other, in order to determine whether any significant difference occurred. For this purpose, six comparisons between original and repeated measurements were performed (three transducers × two ultrasonic parameters). Obtained results are shown in Table 2, indicating that there was no significant difference between the two sets of measurements ($p > 0.05$ for all the considered comparisons).

**Table 1** Obtained values for considered micro-CT and US parameters (mean ± SD)

| Parameter | Value (mean ± SD) |
|---|---|
| trabecular BV/TV | 0.22 ± 0.05 |
| Tb.Th Mean, mm | 0.30 ± 0.05 |
| Tb.Sp Mean, mm | 1.07 ± 0.36 |
| Tb.Th Max, mm | 0.69 ± 0.18 |
| Tb.Sp Max, mm | 2.34 ± 0.49 |
| SMI | 4.18 ± 0.38 |
| BS/TV, $mm^{-1}$ | 0.71 ± 0.25 |
| fractal dimension | 1.89 ± 0.08 |
| Conn.D, $mm^{-3}$ | 0.04 ± 0.02 |
| cortical BV/TV | 0.04 ± 0.01 |
| AIB at 2.25 MHz, dB | −51.02 ± 3.04 |
| AIB at 3.5 MHz, dB | −44.61 ± 3.47 |
| AIB (convex probe), dB | −46.24 ± 3.01 |
| IRC at 2.25 MHz, dB | −46.43 ± 3.37 |
| IRC at 3.5 MHz, dB | −43.45 ± 4.17 |
| IRC (convex probe), dB | −44.58 ± 3.84 |


*IET Sci. Meas. Technol.*, 2016, Vol. 10, Iss. 3, pp. 193–199

**Table 2** Results of the first and the second set of measurements performed by different operators on the same sample

| US parameter | Transducer | 1° measurement set (mean ± SD) | 2° measurement set (mean ± SD) | $p$ |
|---|---|---|---|---|
| AIB | single-element 2.25 MHz | −51.02 ± 3.04 | −51.21 ± 2.63 | 0.82 |
| | single-element 3.5 MHz | −44.61 ± 3.47 | −45.00 ± 3.51 | 0.71 |
| | convex probe | −46.24 ± 3.01 | −46.01 ± 3.01 | 0.83 |
| IRC | single-element 2.25 MHz | −46.43 ± 3.37 | −46.28 ± 3.07 | 0.89 |
| | single-element 3.5 MHz | −43.45 ± 4.17 | −41.96 ± 3.49 | 0.15 |
| | convex probe | −44.58 ± 3.84 | −44.53 ± 3.91 | 0.96 |

**Table 3** Linear correlation coefficients ($r$) between micro-CT and US parameters measured with the 2.25 MHz single-element US transducer

| Micro-CT parameter | AIB | IRC |
|---|---|---|
| trabecular BV/TV | −0.60[a] | −0.22 |
| Tb.Th Mean | −0.40[b] | −0.01 |
| Tb.Sp Mean | −0.48[c] | −0.20 |
| Tb.Th Max | −0.30 | −0.16 |
| Tb.Sp Max | −0.41[b] | −0.10 |
| SMI | −0.29 | −0.17 |
| BS/TV | −0.46[b] | −0.04 |
| fractal dimension | −0.30 | −0.08 |
| Conn.D | −0.20 | −0.03 |
| cortical BV/TV | −0.05 | −0.54[c] |

[a] $p < 0.001$
[b] $p < 0.05$
[c] $p < 0.01$

Therefore, the results reported and discussed in the rest of the paper are referred to the first measurement set.

Pearson's linear correlation coefficients ($r$) between US parameters and micro-CT ones were also calculated for each utilised single-element US transducer (Tables 3 and 4) and for the convex probe (Table 5).

Values shown in Table 3, obtained employing a 2.25 MHz US transducer, are similar to those reported in our preliminary work [43] and they also confirm some previous results documenting appreciable linear correlations between AIB and trabecular structure properties [38]. In particular, the negative correlation between AIB and trabecular BV/TV ($r = -0.60$) indicates that the greater the density of the trabecular region, the smaller the intensity of the backscattered US signal. In fact, when bone density becomes lower, US signals progressively detect more 'discontinuities' in the trabecular structure, as further confirmed by the positive correlations found between AIB and trabecular spacing parameters ($r = 0.48$ with Tb.Sp Mean and $r = 0.41$ with Tb.Sp Max). On the other hand, IRC showed the highest correlation ($r = 0.54$) with cortical BV/TV and the positive sign indicates that the intensity of reflected US signals increases with cortical bone density.

**Table 4** Linear correlation coefficients ($r$) between micro-CT and US parameters measured with the 3.5 MHz single-element US transducer

| Micro-CT parameter | AIB | IRC |
|---|---|---|
| trabecular BV/TV | −0.80[a] | −0.17 |
| Tb.Th Mean | −0.50[b] | −0.04 |
| Tb.Sp Mean | −0.52[b] | −0.20 |
| Tb.Th Max | −0.36 | −0.17 |
| Tb.Sp Max | −0.56[b] | −0.03 |
| SMI | −0.04 | −0.17 |
| BS/TV | −0.69[a] | −0.06 |
| fractal dimension | −0.15 | −0.04 |
| Conn.D | −0.32 | −0.17 |
| cortical BV/TV | −0.28 | −0.57[b] |

[a] $p < 0.001$
[b] $p < 0.01$
[c] $p < 0.05$

**Table 5** Linear correlation coefficients ($r$) between micro-CT and US parameters measured with the convex echographic probe

| Micro-CT parameter | AIB | IRC |
|---|---|---|
| trabecular BV/TV | −0.71[a] | −0.32 |
| Tb.Th Mean | −0.47[b] | −0.04 |
| Tb.Sp Mean | −0.56[b] | −0.31 |
| Tb.Th Max | −0.15 | −0.10 |
| Tb.Sp Max | −0.34 | −0.06 |
| SMI | −0.55[b] | −0.18 |
| BS/TV | −0.72[a] | −0.39[c] |
| fractal dimension | −0.67[a] | −0.35 |
| Conn.D | −0.43[c] | −0.43[c] |
| cortical BV/TV | −0.01 | −0.47[b] |

[a] $p < 0.001$
[b] $p < 0.01$
[c] $p < 0.05$

These findings were qualitatively confirmed by the results of the US acquisitions carried out through a 3.5 MHz transducer (Table 4). In this case, the correlations were typically somewhat stronger with respect to those reported in Table 3, especially for trabecular BV/TV ($r = -0.80$), and this was an expected effect of the increased US frequency, which is associated with a better spatial resolution [38, 52] and with increased backscattering phenomena due to the reduced ratio between acoustic wavelength and trabecular pore size [53].

Very similar correlations were obtained also when a clinically available 128-element convex echographic probe operating at 3.5 MHz was employed for femoral head characterisation (Table 5). The most significant differences observed with respect to the use of a single-element US transducer centred at the same frequency were represented by the higher correlations found for AIB with SMI ($r = 0.55$) and fractal dimension ($r = -0.67$). This positive effect can be due to the combination of two factors: (i) the convex probe bandwidth is wider compared with that of the corresponding single-element transducer; (ii) the electronic focusing of the US beam operated by the echographic probe is more effective than the intrinsic focusing of the employed single-element transducers.

Anyway, correlation data reported in Table 5 demonstrate once more that AIB, which was computed from the US signal segment due to trabecular backscatter, is correlated with trabecular region properties as quantified by micro-CT parameters, whereas IRC, which was computed from the US signal segment due to the reflection produced by the discontinuity between cartilage and cortical bone, is better correlated with bone density of the cortical layer.

It can be observed that we always found good and statistically significant correlations between AIB and trabecular BV/TV (see the corresponding values in Tables 3–5). In particular, as it can be seen from the data reported in Fig. 6, the distributions of trabecular BV/TV and AIB values computed from convex probe acquisitions followed the same trend, with AIB being able to detect important changes in trabecular BV/TV while resulting independent from the insonification angle. Analogous results were found when single-element transducers were employed, further confirming the strong relationship between AIB and trabecular BV/TV, which encourages a prompt clinical translation of the proposed approach.

Preliminary tests confirmed that about half of the femoral head volume was easily accessible during 'in-vivo' echographic acquisitions. Since the femoral head is directly connected to the femoral neck, which is one of the reference axial sites for osteoporosis diagnosis, the availability of additional information about the status of its internal structure (not accessible for DXA investigations) has a potential to improve the clinical management of this pathology.

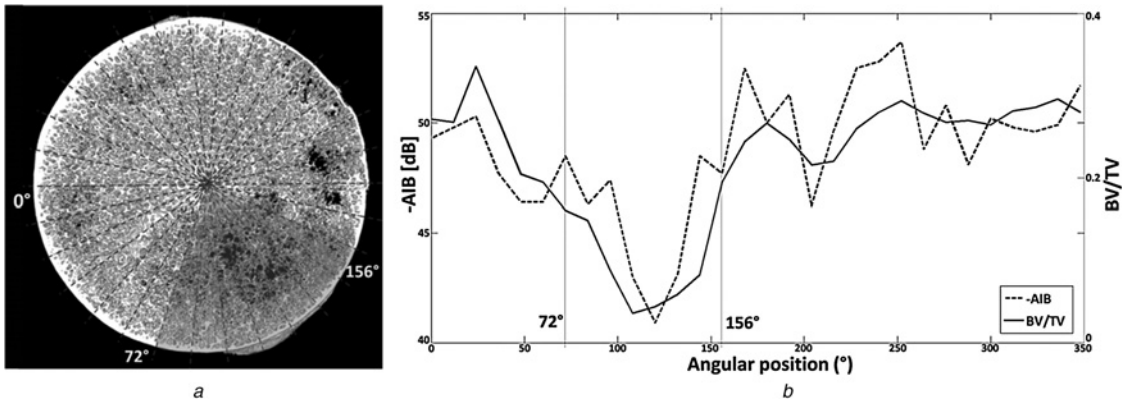


**Fig. 6** *Micro-CT reconstruction of the bone tissue and AIB and trabecular BV/TV values as a function of the insonification direction*

*a* Micro-CT reconstruction of the bone tissue in the sample largest transversal section. The dotted lines represent the 30 angular positions corresponding to the insonification directions during the US acquisitions. The highlighted region between 72° and 156° is characterised by the presence of a high reduction of trabecular bone density

*b* AIB and trabecular BV/TV values as a function of the insonification direction (AIB values were computed from convex probe data). It can be noted that AIB is able to effectively follow the trend of trabecular BV/TV

Actually, the main difference between a real clinical acquisition on a patient and the experimental conditions of the present study is represented by the presence of soft tissues between the US probe and the target bone surface. However, the amount of intervening soft tissue thickness should result in an increased acoustic attenuation, which could be compensated by appropriate settings of echographic device parameters, such as power, gain, focus, time-gain compensation and mechanical index.

Furthermore, the considered anatomical site is characterised by a limited variation of soft tissue thickness as a function of patient physical structure and body mass index. For instance, such variations are much larger for abdominal organs, but this has not prevented the development of US methods for quantitative transabdominal measurements, including in particular a recently introduced approach for osteoporosis diagnosis on lumbar vertebrae [16]. In the case of femoral head acquisitions, it is reasonable to expect a very narrow range of soft tissue thickness variability, at least thanks to the possibility of suitably calibrating the pressure exerted on the probe. Consequently, the reliability of the measurements should be preserved.

Nevertheless, before the actual translation of the proposed approach to clinical routine facilities, further studies will require the investigation of additional US parameters, in order to establish more specific relationships with single micro-CT outputs, as well as the verification of reported findings on a statistically significant number of bone samples and their 'in-vivo' validation through dedicated clinical trials.

## 4 Conclusion

The correlations between two QUS parameters (AIB and IRC) and bone structure properties as quantified by micro-CT were investigated 'in vitro' on a whole human femoral head, employing both single-element US transducers and a clinically available 128-element echographic probe.

Obtained results showed that AIB was strongly correlated with trabecular network properties ($|r|$ up to 0.80) and IRC had appreciable linear correlations with cortical bone density ($|r|$ up to 0.57). The documented agreement between single-element transducers and echographic probe, combined with the innovative approach of considering the entire femoral head in its physiological shape with all its components (cartilage, cortical layer, trabecular region), encourages the clinical translation of the proposed approach as a possible new method for early osteoporosis diagnosis.

## 5 Acknowledgments

This study is an expanded version from 2014 Imeko TC13 – General co-Chairs: A. Lay-Ekuakille and R. Summers. This work was partially funded by FESR P.O. Apulia Region 2007-2013 – Action 1.2.4 (grant no. 3Q5AX31: ECHOLIGHT Project).

## 6 References

1 Pike, C., Birnbaum, H.G., Schiller, M., *et al.*: 'Economic burden of privately insured non-vertebral fracture patients with osteoporosis over a 2-year period in the US', *Osteoporos. Int.*, 2011, **22**, pp. 47–56
2 Brenneman, S.K., Barret-Connor, E., Sajjan, S., *et al.*: 'Impact of recent fracture on health-related quality of life in postmenopausal women', *J. Bone Miner. Res.*, 2006, **21**, (6), pp. 809–816
3 Liu, J.M., Ning, G., Chen, J.L.: 'Osteoporotic fractures in Asia: risk factors and strategies for prevention', *J. Bone Miner. Metab.*, 2007, **25**, pp. 1–5
4 Marin, F., Gonzalez-Macias, J., Diez-Perez, A., *et al.*: 'Relationship between bone quantitative ultrasound and fractures: a meta-analysis', *J. Bone Miner. Res.*, 2006, **21**, pp. 1126–1135
5 Liu, J.M., Ma, L.Y., Bi, Y.F., *et al.*: 'A population-based study examining calcaneus quantitative ultrasound and its optimal cut-points to discriminate osteoporotic fractures among 9352 Chinese women and men', *J. Clin. Endorinol. Metab.*, 2012, **97**, pp. 800–809
6 Baim, S., Leslie, W.D.: 'Assessment of fracture risk', *Curr. Osteoporos. Rep.*, 2012, **10**, pp. 28–41
7 Link, T.M.: 'Osteoporosis imaging: state of the art and advanced imaging', *Radiology*, 2012, **263**, pp. 3–17
8 Nayak, S., Olkin, I., Liu, H., *et al.*: 'Meta-analysis: accuracy of quantitative ultrasound for identifying patients with osteoporosis', *Ann. Intern. Med.*, 2006, **144**, pp. 832–841
9 Pais, R., Campean, R., Simon, S.-P., *et al.*: 'Accuracy of quantitative ultrasound parameters in the diagnosis of osteoporosis', *Cent. Eur. J. Med.*, 2010, **5**, pp. 478–485
10 Schnitzer, T.J., Wysocki, N., Barkema, D., *et al.*: 'Calcaneal quantitative ultrasound compared with hip and femoral neck dual-energy X-ray absorptiometry in people with a spinal cord injury', *PM R*, 2012, **4**, pp. 748–755
11 Brambilla, M., De Mauri, A., Leva, L., *et al.*: 'Cumulative radiation dose from medical imaging in chronic adult patients', *Am. J. Med.*, 2013, **126**, pp. 480–486
12 Picano, E., Matucci-Cerinic, M.: 'Unnecessary radiation exposure from medical imaging in the rheumatology patient', *Rheumatology*, 2011, **50**, pp. 1537–1539
13 Picano, E., Vano, E.: 'Radiation exposure as an occupational hazard', *Eurointervention*, 2012, **8**, pp. 649–653
14 Semelka, R.C., Armao, D.M., Elias, J. Jr., *et al.*: 'The information imperative: is it time for an informed consent process explaining the risks of medical radiation?', *Radiology*, 2012, **262**, pp. 15–18
15 Compston, J.E., Cooper, C., Kanis, J.A.: 'Bone densitometry in clinical practice', *BMJ*, 1995, **310**, pp. 1507–1510
16 Conversano, F., Franchini, R., Greco, A., *et al.*: 'A novel ultrasound methodology for estimating spine mineral density', *Ultrasound Med. Biol.*, 2015, **41**, (1), pp. 281–300
17 Silva, B.C., Walker, M.D., Abraham, A., *et al.*: 'Trabecular bone score is associated with volumetric bone density and microarchitecture as assessed by central QCT and HRpQCT in Chinese-American and white women', *J. Clin. Densitom.*, 2013, **16**, pp. 554–561
18 Hans, D., Barthe, N., Boutroy, S., *et al.*: 'Correlations between trabecular bone score, measured using anteroposterior dual-energy X-ray absorptiometry acquisition, and 3-dimensional parameters of bone microarchitecture: an experimental study on human cadaver vertebrae', *J. Clin. Densitom.*, 2011, **14**, (3), pp. 302–312
19 Pisani, P., Renna, M.D., Conversano, F., *et al.*: 'Screening and early diagnosis of osteoporosis through X-ray and ultrasound based techniques', *World J. Radiol.*, 2013, **5**, (11), pp. 398–410

20 Casciaro, S., Pisani, P., Soloperto, G., *et al.*: 'An innovative ultrasound signal processing technique to selectively detect nanosized contrast agents in echographic images', *IEEE Trans. Instrum. Meas.*, 2015, **64**, (8), pp. 2136–2145
21 Casciaro, S., Conversano, F., Casciaro, E., *et al.*: 'Automatic evaluation of progression angle and fetal head station through intrapartum echographic monitoring', *Comput. Math. Methods Med.*, 2013, p. 8, Article ID 278978
22 Chiriacò, F., Conversano, F., Soloperto, G., *et al.*: 'Epithelial cells biocompatibility of silica nanospheres for contrast enhanced ultrasound molecular imaging', *J. Nanoparticle Res.*, 2013, **15**, (7), pp. 1–13
23 Soloperto, G., Conversano, F., Greco, A., *et al.*: 'Advanced spectral analyses for real time automatic echographic tissue-typing of simulated tumour masses at different compression stages', *IEEE Trans. Ultrason. Ferroelectr. Freq. Control*, 2012, **59**, (12), pp. 2692–2701
24 Conversano, F., Soloperto, G., Greco, A., *et al.*: 'Echographic detectability of optoacoustic signals from low concentration PEG-coated gold nanorods', *Int. J. Nanomed.*, 2012, **7**, pp. 4373–4389
25 Conversano, F., Greco, A., Casciaro, E., *et al.*: 'Harmonic ultrasound imaging of nanosized contrast agents for multimodal molecular diagnoses', *IEEE Trans. Instrum. Meas.*, 2012, **61**, (7), pp. 1848–1856
26 Conversano, F., Franchini, R., Lay-Ekuakille, A., *et al.*: 'In vitro evaluation and theoretical modeling of the dissolution behavior of a microbubble contrast agent for ultrasound imaging', *IEEE Sens. J.*, 2012, **12**, (3), pp. 496–503
27 Conversano, F., Casciaro, E., Franchini, R., *et al.*: 'A quantitative and automatic echographic method for real-time localization of endovascular devices', *IEEE Trans. Ultrason. Ferroelectr. Freq. Control*, 2011, **58**, (10), pp. 2107–2117
28 Casciaro, S., Conversano, F., Musio, S., *et al.*: 'Full experimental modelling of a liver tissue mimicking phantom for medical ultrasound studies employing different hydrogels', *J. Mater. Sci., Mater. Med.*, 2009, **20**, (4), pp. 983–989
29 Demitri, C., Sannino, A., Conversano, F., *et al.*: 'Hydrogel based tissue mimicking phantom for in-vitro ultrasound contrast agents studies', *J. Biomed. Mater. Res. B, Appl. Biomater.*, 2008, **87**, (2), pp. 338–345
30 Casciaro, S., Palmizio Errico, R., Conversano, F., *et al.*: 'Experimental investigations of nonlinearities and destruction mechanisms of an experimental phospholipid-based ultrasound contrast agent', *Invest. Radiol.*, 2007, **42**, (2), pp. 95–104
31 Njeh, C.F., Boivin, C.M., Langton, C.M.: 'The role of ultrasound in the assessment of osteoporosis: a review', *Osteoporos. Int.*, 1997, **7**, (1), pp. 7–22
32 Prins, S.H., Jorgensen, H.L., Jorgensen, L.V., *et al.*: 'The role of quantitative ultrasound in the assessment of bone: a review', *Clin. Physiol.*, 1998, **18**, (1), pp. 3–17
33 Conversano, F., Casciaro, E., Franchini, R., *et al.*: 'A new ultrasonic method for lumbar spine densitometry'. Proc. IEEE Int. Ultrasonics Symp. (IUS), Prague, Czech Republic, July 2013, pp. 1809–1812
34 Bauer, D.C., Gluer, C.C., Genant, H.K., *et al.*: 'Quantitative ultrasound and vertebral fracture in postmenopausal women. Fracture Intervention Trial Research Group', *J. Bone Miner. Res.*, 1995, **10**, pp. 353–358
35 Gluer, C.C., Eastell, R., Reid, D.M., *et al.*: 'Association of five quantitative ultrasound devices and bone densitometry with osteoporotic vertebral fractures in a population-based sample: the OPUS study', *J. Bone Miner. Res.*, 2004, **19**, pp. 782–793
36 Guglielmi, G., de Terlizzi, F.: 'Quantitative ultrasound in the assessment of osteoporosis', *Eur. J. Radiol.*, 2009, **71**, pp. 425–431
37 Wear, K.A., Nagaraja, S., Dreher, M., *et al.*: 'Relationships of quantitative ultrasound parameters with cancellous bone microstructure in human calcaneus in vitro', *J. Acoust. Soc. Am.*, 2012, **131**, pp. 1605–1612
38 Hoffmeister, B.K., Johnson, D.P., Janeski, J.A., *et al.*: 'Ultrasonic characterization of human cancellous bone in vitro using three different apparent backscatter parameters in the frequency range 0.6–15 MHz', *IEEE Trans. Ultrason. Ferroelectr. Freq. Control.*, 2008, **55**, pp. 1442–1452
39 Jiang, Y.-Q., Liu, C.-C., Li, R.-Y., *et al.*: 'Analysis of apparent integrated backscatter coefficient and backscatter spectral centroid shift in calcaneus in vivo for the ultrasonic evaluation of osteoporosis', *Ultrasound Med. Biol.*, 2014, **40**, pp. 1307–1317
40 Karjalainen, J.P., Toyras, J., Riekkinen, O., *et al.*: 'Ultrasound backscatter imaging provides frequency-dependent information on structure, composition and mechanical properties of human trabecular bone', *Ultrasound Med. Biol.*, 2009, **35**, pp. 1376–1384
41 Karjalainen, J.P., Riekkinen, O., Toyras, J., *et al.*: 'Multi-site bone ultrasound measurements in elderly women with and without previous hip fractures', *Osteoporos. Int.*, 2012, **23**, pp. 1287–1295
42 Hoffmeister, B.K., Wilson, A.R., Gilbert, M.J., *et al.*: 'A backscatter difference technique for ultrasonic bone assessment', *J. Acoust. Soc. Am.*, 2012, **132**, pp. 4069–4076
43 Peccarisi, M., De Marco, T., Spedicato, L., *et al.*: 'In vitro ultrasound characterization of human proximal femur microstructure and comparison with micro-CT data'. Proc. 3rd Imeko TC13 Symp. on Measurements in Biology and Medicine 'New Frontiers in Biomedical Measurements', Lecce, Italy, April 2014, pp. 62–66
44 Hakulinen, M.A., Toyras, J., Saarakkala, S., *et al.*: 'Ability of ultrasound backscattering to predict mechanical properties of bovine trabecular bone', *Ultrasound Med. Biol.*, 2004, **30**, (7), pp. 919–927
45 Laugier, P., Haiat, G.: 'Bone quantitative ultrasound' (Springer, 2010)
46 Buie, H.R., Campbell, G.M., Klinck, R.J., *et al.*: 'Automatic segmentation of cortical and trabecular compartments based on a dual threshold technique for in vivo micro-CT bone analysis', *Bone*, 2007, **41**, (4), pp. 505–515
47 Doube, M., Klosowski, M.M., Arganda-Carreras, I., *et al.*: 'BoneJ: free and extensible bone image analysis in ImageJ', *Bone*, 2010, **47**, (6), pp. 1076–1079
48 Dougherty, R., Kunzelmann, K.: 'Computing local thickness of 3D structures with ImageJ', *Microsc. Microanal.*, 2007, **13**, (2), pp. 1678–1679
49 Hildebrand, T., Ruegsegger, P.: 'Quantification of bone microarchitecture with the structure model index', *Comput. Methods Biomech. Biomed. Eng.*, 1997, **1**, (1), pp. 15–23
50 Fazzalari, N.L., Parkinson, I.H.: 'Fractal dimension and architecture of trabecular bone', *J. Pathol.*, 1996, **178**, (1), pp. 100–105
51 Odgaard, A., Gundersen, H.J.S.: 'Quantification of connectivity in cancellous bone, with special emphasis on 3-D reconstructions', *Bone*, 1993, **14**, (2), pp. 173–182
52 Hakulinen, M.A., Day, J.S., Töyräs, J., *et al.*: 'Ultrasonic characterization of human trabecular bone microstructure', *Phys. Med. Biol.*, 2006, **51**, (6), pp. 1633–1648
53 Hakulinen, M.A., Day, J.S., Juha, T., *et al.*: 'Prediction of density and mechanical properties of human trabecular bone in vitro by using ultrasound transmission and backscattering measurements at 0.2–6.7 MHz frequency range', *Phys. Med. Biol.*, 2005, **50**, (8), pp. 1629–1642